JOURNAL OF SPACECRAFT AND ROCKETS
Vol. 41, No. 6, November–December 2004

Engineering Estimates of Normal Loads on Slender Airbreathing Bodies

Prabhu Ramachandran,* S. C. Rajan,† and S. Santhakumar‡
Indian Institute of Technology—Madras, Chennai 600 036, India

A method is developed to obtain quick engineering estimates for the normal load on slender airbreathing shapes. Estimates of the normal load can be obtained using a Trefftz plane analysis. This computation, although two-dimensional and subsonic, agrees fairly well with experimental data (from NASA and AGARD) for three-dimensional slender bodies in supersonic flows. The computational technique is simple and extremely fast.

Nomenclature

A	=	area of cross section, m^2
AR	=	aspect ratio of body or wing
$b1$, $b2$	=	limits of the span of the body, m
F	=	force of fluid on body, kg m/s^2
F'	=	force of body on fluid, kg m/s^2
$\boldsymbol{i}, \boldsymbol{j}, \boldsymbol{k}$	=	Cartesian unit vectors along x, y, z
M	=	Mach number
$\boldsymbol{n}$	=	unit outward normal direction
p	=	pressure, Pa
S	=	surface area, m^2
s	=	arc length along curve, m
$s1$, $s2$	=	arc lengths at points 1 and 2, m
V	=	velocity magnitude, m/s
$\boldsymbol{V}$	=	velocity vector, m/s
u, v, w	=	perturbation velocities along x, y, z, m/s
x, y, z	=	Cartesian coordinate axes, m
α	=	angle of attack, deg
γ	=	intensity of vorticity of the sheet, m/s
ρ	=	density, kg/m^3
ϕ	=	perturbation potential, m^2/s

Subscripts

x, y, z	=	component along Cartesian coordinate
1	=	values at plane 1
2	=	values at plane 2
∞	=	freestream

Introduction

THE present work seeks to develop and evaluate a simple technique to compute engineering estimates of the normal load for slender airbreathing shapes at small angles of attack. The flowfield itself could be supersonic (nearly up to a Mach number of 4.0). For a slender body, we define the aspect ratio AR as defined for wings. For example, for a circular duct of diameter D and length L the aspect ratio is defined as the square of diameter divided by planform area and is equal to D/L. It is known[1,2] that for low-aspect-ratio bodies the normal load can be effectively computed from the shape and intensity of vorticity of the trailing vortex sheet in the Trefftz plane. The Trefftz plane is an idealized plane far downstream of the body. This plane contains the trailing vorticity of the body. It is possible to estimate the load on the body using this trailing vorticity distribution. Rajan and Shashidhar[2] worked out an exact leading term solution for low-aspect-ratio wings using a Trefftz plane analysis. These results are valid for finite but low-aspect-ratio wings.

For slender, low-aspect-ratio bodies, the vorticity distribution in the Trefftz plane is the result of the crossflow. Hence, it is the crossflow that is responsible for the normal load and not the axial flow. Even if the flow is supersonic, for small angles of attack the crossflow is only subsonic. For higher Mach numbers the crossflow Mach number can be treated as subsonic and compressible. Because of this, it is possible to use a two-dimensional Trefftz plane analysis and compute the normal load with some confidence. Because the analysis is two dimensional, the method is very efficient and easy to apply. The computed results are compared with the experimental data of AGARD[3] and NASA.[4–6] The NASA results are for various missile shapes at supersonic and subsonic Mach numbers. The computed results agree fairly well with the experimental results.

Mathematical Details

In Fig. 1, a lifting body and the accompanying trailing vortex sheet shed by it are shown. The body represents a duct with a fan inside it. If the fan is stopped, the body behaves like a closed body and if running behaves like an airbreathing body. The body and wake are enclosed by a control volume whose sides are part of a stream-tube. Planes 1 and 2 are located respectively far upstream and far downstream of the body. Plane 2 is the Trefftz plane when located far downstream at infinity. In Fig. 2, a sample intersection of the trailing vortex system and plane 2 is shown for a particular body cross-section shape. The region O_v is the region outside the vortex sheet, and I_v is the one inside the vortex sheet.

For low-aspect-ratio bodies in incompressible flow, the shape of the vortex sheet in the Trefftz plane can be assumed to be the same as the cross-sectional shape of the body at the axial location where the cross-sectional area becomes maximum. For the body shown in Fig. 1, the intensity of the vorticity at the Trefftz plane is assumed to be the same as the corresponding two-dimensional surface vorticity for the cross-sectional flow at the location where the cross-sectional area of the body becomes maximum. Using this distribution of vorticity, the normal load on the body can be computed as detailed in the following.

Applying the conservation-of-mass equation to the control volume shown in Fig. 1, we have

$$\int_1 \rho(V_\infty \cos\alpha + u_1)\boldsymbol{i}\cdot\boldsymbol{n}\,\mathrm{d}S + \int_2 \rho(V_\infty \cos\alpha + u_2)\boldsymbol{i}\cdot\boldsymbol{n}\,\mathrm{d}S = 0$$

where the numbers 1 and 2 on the integral indicate that they are to be evaluated on the planes 1 and 2. For points on plane 1, $\boldsymbol{n} = -\boldsymbol{i}$, and $\boldsymbol{n} = \boldsymbol{i}$ for points on plane 2. u_1 and u_2 are x components of the perturbation velocities at planes 1 and 2, respectively. Because the sides of the control volume are a part of a stream tube, there can be no flow of mass or momentum across them. If planes 1 and 2 extend

Received 25 June 2003; revision received 9 January 2004; accepted for publication 26 January 2004.

*Graduate Student, Department of Aerospace Engineering.
†Assistant Professor, Department of Aerospace Engineering.
‡Professor, Department of Aerospace Engineering.

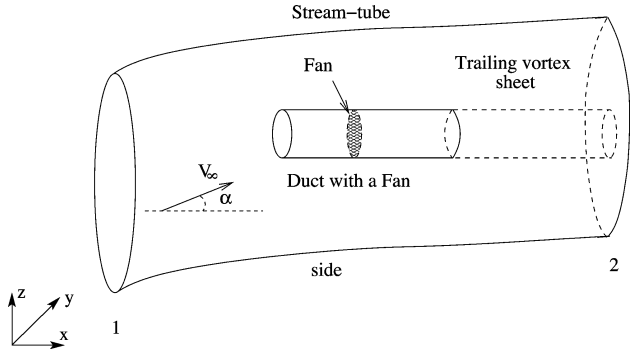

Fig. 1 Duct with a fan enclosed by a control volume considered for the calculation of the normal load.

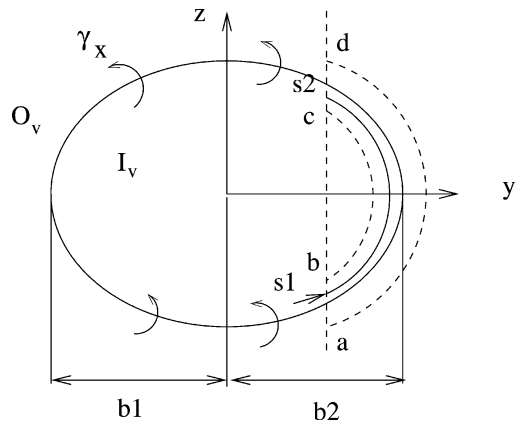

Fig. 2 Vortex sheet in the Trefftz plane.

far upstream and downstream, respectively, it is easy to see that the preceding equation reduces to

$$\int_1 \rho V_\infty \cos\alpha \, dS = \int_2 \rho(V_\infty \cos\alpha + u_2)\, dS \tag{1}$$

The perturbation u_2 in the wake of the body is nonzero in general. This can happen if the body is solid or has a fan. For example, if the body is solid, $u_2 = -V_\infty \cos\alpha$, in the wake of the body. If the body is open, then $u_2 = 0$, and if there is a fan or a jet inside u_2 can be some nonzero value.

Now applying the momentum theorem along the z direction to the chosen control volume, we can see that the force of the lifting body on the flow in the z direction is

$$F_z' = \int_1 \rho(\boldsymbol{V}\cdot\boldsymbol{n})(\boldsymbol{V}\cdot\boldsymbol{k})\, dS + \int_2 \rho(\boldsymbol{V}\cdot\boldsymbol{n})(\boldsymbol{V}\cdot\boldsymbol{k})\, dS + \int_{\text{side}} p\boldsymbol{n}\cdot\boldsymbol{k}\, dS$$

It can be easily shown that when the control volume surface is moved very far away from the body the contribution of the pressure integral along the z direction is zero. Simplifying the preceding and noting that for points on the plane 1, $\boldsymbol{n} = -\boldsymbol{i}$ and for points on plane 2, $\boldsymbol{n} = \boldsymbol{i}$, we have

$$F_z' = \int_2 \rho(V_\infty \cos\alpha + u_2)(V_\infty \sin\alpha + w_2)\, dS - \int_1 \rho V_\infty \cos\alpha V_\infty \sin\alpha \, dS$$

where w_2 is the perturbation velocity along the z axis in plane 2. This equation is rearranged as

$$F_z' = \int_2 \rho(V_\infty \cos\alpha + u_2)V_\infty \sin\alpha \, dS - \int_1 \rho V_\infty \cos\alpha V_\infty \sin\alpha \, dS + \int_2 \rho(V_\infty \cos\alpha + u_2)w_2 \, dS$$

Multiplying Eq. (1) with $V_\infty \sin\alpha$, it is clear that the first two integrals in the preceding equation cancel. It is also clear that the force of the fluid on the body is $F_z = -F_z'$. Hence we have

$$F_z = -\int_2 \rho(V_\infty \cos\alpha + u_2)w_2 \, dS \tag{2}$$

The fluid flow outside the trailing vortex system is purely irrotational. Far downstream of the body, the flow is two dimensional. Given this, it is easy to see that outside the trailing vortex system $u_2 = 0$ that is, the perturbation velocity along the x axis far downstream and just outside the trailing vortex system is zero. Thus, u_2 is nonzero only in the wake of the body. Because $w_2 = \partial\phi/\partial z$, Eq. (2) can be written as

$$\begin{aligned} F_z &= -\int_{-\infty}^{\infty} dy \int_{-\infty}^{\infty} \rho(V_\infty \cos\alpha + u_2)\frac{\partial\phi}{\partial z}\, dz \\ &= -\int_{-\infty}^{-b1} dy \int_{-\infty}^{\infty} \rho(V_\infty \cos\alpha + u_2)\frac{\partial\phi}{\partial z}\, dz \\ &\quad -\int_{-b1}^{b2} dy \int_{-\infty}^{\infty} \rho(V_\infty \cos\alpha + u_2)\frac{\partial\phi}{\partial z}\, dz \\ &\quad -\int_{b2}^{\infty} dy \int_{-\infty}^{\infty} \rho(V_\infty \cos\alpha + u_2)\frac{\partial\phi}{\partial z}\, dz \end{aligned}$$

In the first and last integrals it can be seen that $u_2 = 0$; therefore, the first and last integrals can be written as

$$-\rho V_\infty \cos\alpha \int_{-\infty}^{-b1} [\phi(\infty, y, \infty) - \phi(\infty, y, -\infty)]\, dy$$

$$-\rho V_\infty \cos\alpha \int_{b2}^{\infty} [\phi(\infty, y, \infty) - \phi(\infty, y, -\infty)]\, dy$$

It is easy to see that $\phi(\infty, y, \infty) = \phi(\infty, y, -\infty) = 0$. From these observations Eq. (2) can be written as

$$F_z = -\int_{-b1}^{b2} dy \int_{-\infty}^{\infty} \rho(V_\infty \cos\alpha + u_2)\frac{\partial\phi}{\partial z}\, dz \tag{3}$$

In Fig. 2 the vertical dashed line intersects the vortex sheet at points a and d. These are points just outside the sheet, and b and c are corresponding points just inside the vortex sheet. It is known that across a vortex sheet the value of ϕ jumps. Hence the integral in Eq. (3) must be evaluated carefully. Noting that $u_2 = 0$ outside the vortex sheet and that ρ and $V_\infty \cos\alpha$ are constant, this integral can be written as

$$F_z = -\rho V_\infty \cos\alpha \int_{-b1}^{b2} dy \left(\int_{-\infty}^{a} \frac{\partial\phi}{\partial z}\, dz + \int_b^c \frac{\partial\phi}{\partial z}\, dz + \int_d^{\infty} \frac{\partial\phi}{\partial z}\, dz \right) - \rho \int_{-b1}^{b2} dy \int_b^c u_2 \frac{\partial\phi}{\partial z}\, dz \tag{4}$$

It is known that across a vortex sheet the value of ϕ jumps. Therefore $\phi_a \neq \phi_b$, and $\phi_c \neq \phi_d$. Then,

$$\begin{aligned} \int_{-\infty}^{\infty} \frac{\partial\phi}{\partial z}\, dz &= \int_{-\infty}^{a} d\phi + \int_b^c d\phi + \int_d^{\infty} d\phi \\ &= \phi_a + \phi_c - \phi_b - \phi_d \end{aligned} \tag{5}$$

The value of $\phi_a + \phi_c - \phi_b - \phi_d$ can be related to the vorticity of the trailing vortex at the Trefftz plane. As shown in Fig. 2, considering

the closed dotted contour, which passes through points (a, b) and (c, d),

$$\int_a^d \boldsymbol{V}\cdot\boldsymbol{ds} + \int_c^b \boldsymbol{V}\cdot\boldsymbol{ds} = \int_a^d \mathrm{d}\phi + \int_c^b \mathrm{d}\phi$$
$$= \phi_d - \phi_a + \phi_b - \phi_c \tag{6}$$

Also,

$$\int_a^d \boldsymbol{V}\cdot\boldsymbol{ds} + \int_c^b \boldsymbol{V}\cdot\boldsymbol{ds} = \int_{s1}^{s2} \gamma_x\,\boldsymbol{ds} \tag{7}$$

where s is the curvilinear coordinate measured along the vortex sheet, as shown in Fig. 2. The origin for s can be chosen arbitrarily. It can be mentioned that $s1 = s_a = s_b$ and $s2 = s_c = s_d$. From Eqs. (6) and (7) it follows that

$$\phi_d - \phi_a + \phi_b - \phi_c = \int_{s1}^{s2} \gamma_x\,\mathrm{d}s \tag{8}$$

From Eqs. (5) and (8) we find that

$$\int_{-\infty}^{\infty} \frac{\partial\phi}{\partial z}\,\mathrm{d}z = -\int_{s1}^{s2} \gamma_x\,\mathrm{d}s \tag{9}$$

Equation (4) can then be written as

$$F_z = \rho V_\infty \cos\alpha \int_{-b1}^{b2} \mathrm{d}y \int_{s1}^{s2} \gamma_x\,\mathrm{d}s - \rho \int_{-b1}^{b2} \mathrm{d}y \int_b^c u_2 \frac{\partial\phi}{\partial z}\,\mathrm{d}z \tag{10}$$

Note that

$$\int_{s1}^{s2} \gamma_x\,\mathrm{d}s$$

is a function of y and that the second integral is to be evaluated only inside the area enclosed by the vortex sheet. Hence using Eq. (10) one can compute the normal load on a duct by using the vorticity distribution in the Trefftz plane. The distribution and value of u_2 in the wake must be known.

For example, consider the case of an open duct such that there is free axial flow through the body. Assuming that $u_2 = 0$ inside the vortex sheet, the normal force on the duct is given by

$$F_z = \rho V_\infty \cos\alpha \int_{-b1}^{b2} \mathrm{d}y \int_{s1}^{s2} \gamma_x\,\mathrm{d}s$$

Consider a solid body having cross-sectional area A_s with no internal flow. It can be seen that for this case, $u_2 = -V_\infty \cos\alpha$. It can also be easily seen that inside the trailing vortex sheet at $x = \infty$ there is no flow. Hence the perturbation w_2 inside the body becomes $-V_\infty \sin\alpha$. Hence,

$$F_z = \rho V_\infty \cos\alpha \int_{-b1}^{b2} \mathrm{d}y \int_{s1}^{s2} \gamma_x\,\mathrm{d}s - \rho V_\infty^2 \cos\alpha \sin\alpha A_s$$

For a circular shape this results in the load of a solid cylinder being half of that of a circular duct, which is open to the flow.

Methodology

To compute the normal load on an arbitrary slender shape, the vorticity distribution (intensity of γ) in the Trefftz plane is required. To compute this for slender three-dimensional airbreathing shapes, the axial location where the cross-sectional area enclosed becomes maximum is chosen. Alternatively, the axial view of the body is projected onto the Trefftz plane, and this projected two-dimensional shape is considered. The cylinder having the preceding cross-sectional shape is exposed to uniform flow having speed $V_\infty \sin\alpha$ to obtain the distribution of γ. This reduces the three-dimensional problem to a two dimensional one. For simple cross sections like cylinder and flat plate, the exact solution for γ is known. For complicated shapes the distribution of vorticity can be obtained numerically, using a panel method. Once the intensity of surface vorticity γ is known, the normal load is calculated using Eq. (10).

In the present work a linear vortex panel method is used to compute the γ distribution. The surface is divided into a set of straight panel elements. On a panel, vorticity is distributed linearly. The no-penetration condition is enforced at the center of each panel, which results in a set of linear equations for the unknown γ. The solution of this linear system of equations gives the distribution of γ, the surface vorticity.

It is obvious that this method is insensitive to changes in the actual shape of the body so long as the maximum cross-sectional shape remains the same. It is also clear that this method cannot be used to compute the pitching moment on the body. However, the load computation using the Trefftz plane analysis only requires a two-dimensional geometry and hence is extremely quick. The next section discusses the results obtained for various shapes using the present method and compares them with available experimental data.

Results and Discussion

In this section computational results using the Trefftz plane analysis are presented. The computations are performed for various missile shapes and are compared with experimental data. Experimental data from AGARD[3] and NASA[4–6] are used for comparison. All of the computations are performed using a subsonic method, whereas the experimental data are mostly for supersonic flow.

Comparison with AGARD CP 493 Data

In their AGARD report, Champigny et al.[3] consider a slender missile shape consisting of a central body and two symmetrically located open ducts outside the body. The circumferential location of the ducts is variable, and the cross section of the configuration is shown in Fig. 3. Experimental values of $C_{N\alpha}$ as a function of $(s/D - 1)\cos\beta$ are available. The parameters s, D, and β are given in Fig. 3.

The computations are performed using the present method. Two cases are considered. In the first case $\beta = 0$. With the shape being symmetric, the other duct is at $\beta = 180$ deg. D and s are varied. In the second case considered, s is taken as 2.25 m, and $D = 1.0$ m. β alone is varied from 0 to 45 deg. For both cases the flow through the ducts is assumed to have a constant velocity of $V_\infty \cos\alpha$. The results for these cases are presented in Fig. 4. The experimental value of freestream Mach number M_∞ is 3.2. As can be seen, the agreement is good even though the present analysis is subsonic. These results are of interest because several different geometries (as a result of variation in β and s/D) are considered when obtaining the results.

We check the convergence of the results by considering one of the geometries and recomputing the load after doubling the number of panels. For the case where $\beta = 10$ deg and $s/D = 2.25$, the data shown in Fig. 4 were computed using 450 panels. Let the resulting value of $C_{N\alpha}$ be $C_{N\alpha_2}$. The number of panels are doubled and $C_{N\alpha}$ is recomputed. This value is denoted as $C_{N\alpha_1}$. Because the results

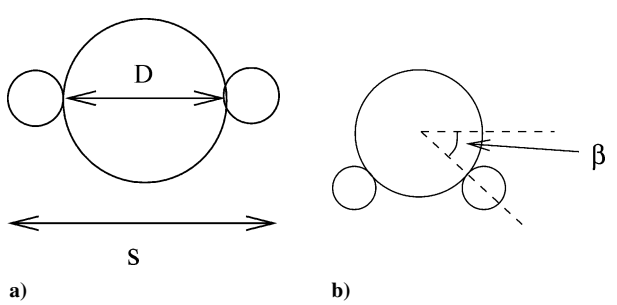

Fig. 3 Various parameters used in the computation of $C_{N\alpha}$ for the missile shapes presented in the AGARD CP 493 report.

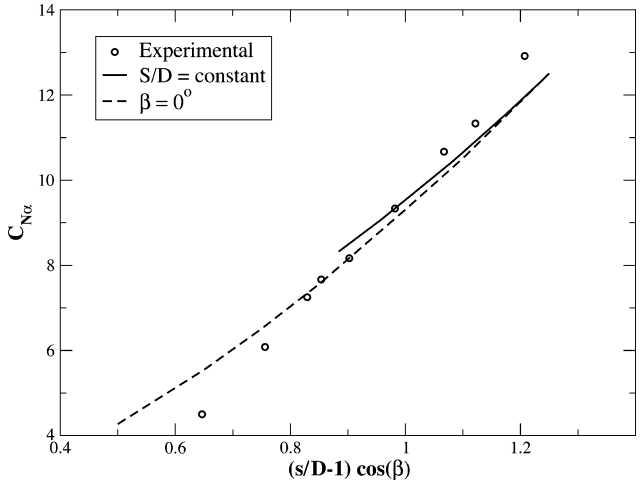

Fig. 4 Computed and experimental $C_{N\alpha}$ for the AGARD CP 493 configurations: ——, plots the case when $s/D = 2.25$ and β is varied and – – –, plots the case where $\beta = 0$ and s/D is varied. The experimental value of $M_\infty = 3.2$.

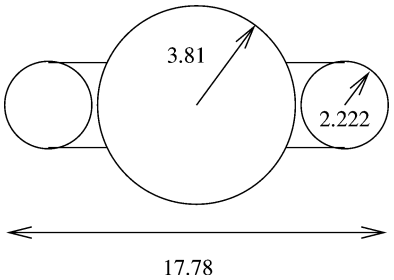

Fig. 5 Simplified B1I1 geometry considered for the computation (all dimensions in centimeters).

used in the figure are from the coarser grid, we compute the coarse grid GCI[7] (grid convergence index) as

$$\mathrm{GCI} = [3r^p/(r^p - 1)]\left[\left(C_{N\alpha_1} - C_{N\alpha_2}\right)\Big/ C_{N\alpha_1}\right] \qquad (11)$$

where $r = 2$ in the present case and p is assumed to be 2. Using this, we find that the GCI = 0.0071, which is very small and shows that for practical purposes the results have indeed converged.

Comparison with NASA Data

The computational results using the Trefftz plane analysis are compared with a few configurations tested by Hayes.[4–6] The NASA reports provide experimental data for various airbreathing missile configurations at supersonic and subsonic speeds. The experimental configurations include twin axisymmetric inlets and two-dimensional inlets. Results for various supersonic Mach numbers ranging from Mach 2.5 to 3.95 are presented. There are several geometries for which experimental data are available. Only a few of them are considered in this work.

The first case considered is a cylindrical solid body with twin axisymmetric inlets that are at an angle of 90 deg with respect to the vertical. As per the NASA data, the case has been referred to as B1I1. The actual three-dimensional shapes of the NASA configurations are fairly complex. The present computations use a simplified version of the NASA geometry. The simplified geometry considered for the axisymmetric inlet case (B1I1 configuration) is shown in Fig. 5. For this case the two-dimensional results are shown in Fig. 6. Two computations are performed: one with the ducts fully open and the other fully closed. The mass flow rate through the body was unavailable, and hence these two plots are presented. As can be seen, the agreement is fairly good.

To show convergence, the number of panels are doubled (from 210 to 420 panels) for the $\alpha = 8$ deg case with no-through flow and

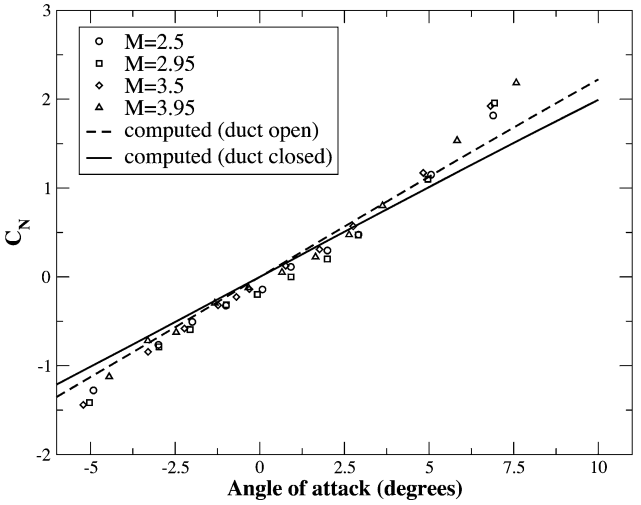

Fig. 6 Computed and experimental results for C_N vs α for the NASA B1I1 configuration with the ducts as shown in Fig. 5. The experimental results are for various supersonic Mach numbers.

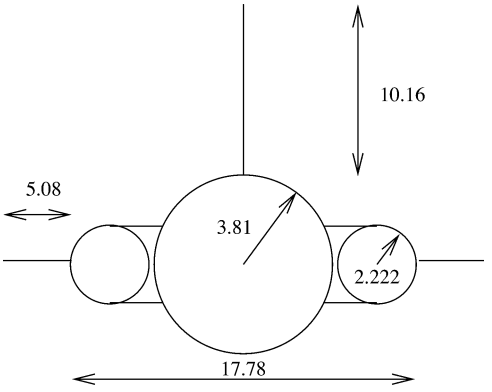

Fig. 7 Cross section of the NASA B1I1T1 configuration (all dimensions in centimeters).

the coarse grid GCI is computed using Eq. (11) with $C_{N\alpha}$ replaced by C_N. It is found that the GCI = 0.000224, which is very small, indicating good convergence.

In a similar fashion the results for the B1I1T1 configuration are also presented. The cross section of the missile shape is as shown in Fig. 7. The results are presented in Fig. 8. For this case the GCI = 0.000814, again indicating good convergence. The GCI is computed by increasing the number of panels from 330 to 660 panels.

As can be seen from the results, the computed C_N values are higher than the experimental values. This is because in the actual three-dimensional geometry the tail is in the rear section of the body and in the wake of the vortices shed by the engine. Therefore, the tail will not generate a significant amount of lift. However, the present method cannot differentiate between such a tail and one that extends up to the nose. The computation will therefore overpredict the lift. The two-dimensional analysis is incapable of modeling this. However, the correct trend in the load seems to have been captured, and the computations should serve as a reasonable engineering estimate for the load.

The case having twin two-dimensional inlets at 90 deg with respect to the vertical is considered next. The geometry considered is shown in Fig. 9. The results of the present method are shown in Fig. 10. For this case the coarse grid GCI = 0.004346 is obtained by doubling the panels from 244 to 488 panels. The GCI is very small (less than 0.5%) and again indicates good convergence.

The agreement in this case is not as good as the case of the axisymmetric inlet case. The experimental values are larger than the computed ones. This is because of separation of the flow at the

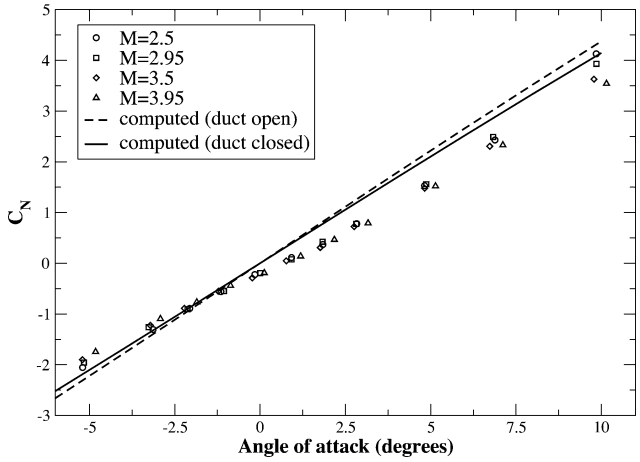

Fig. 8 Computed and experimental results for C_N vs α for the NASA B1I1T1 configuration with the ducts as shown in Fig. 7. The experimental results are for various supersonic Mach numbers.

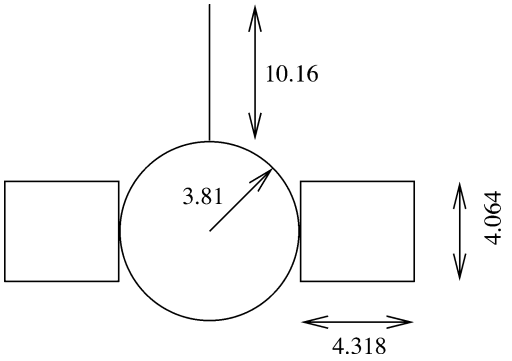

Fig. 9 Simplified B1I2 geometry considered for the computation (all dimensions in centimeters).

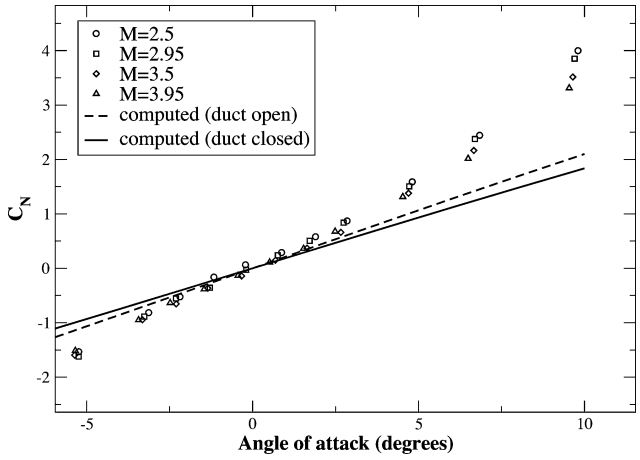

Fig. 10 Computed and experimental results for C_N vs α for the NASA B1I2 configuration with the ducts as shown in Fig. 9. The experimental results are for different supersonic Mach numbers.

sharp edges along the inlet sides. The simple Trefftz plane analysis presented here does not take into consideration the separation of the flow.

Finally, the results for the B1I2T1 configuration as per the NASA report are also presented next. The configuration of the missile shape is shown in Fig. 11. The results are presented in Fig. 12. The coarse grid GCI = 0.0041015 is obtained by doubling the panels from 336 to 672 panels. This again indicates good convergence.

The results are in good agreement here because of the effect of the tail. In the experimental case, the tail is in the wake of the engine shed

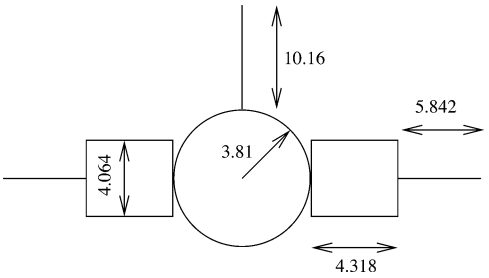

Fig. 11 Cross section of the NASA B1I2T1 configuration (all dimensions in centimeters).

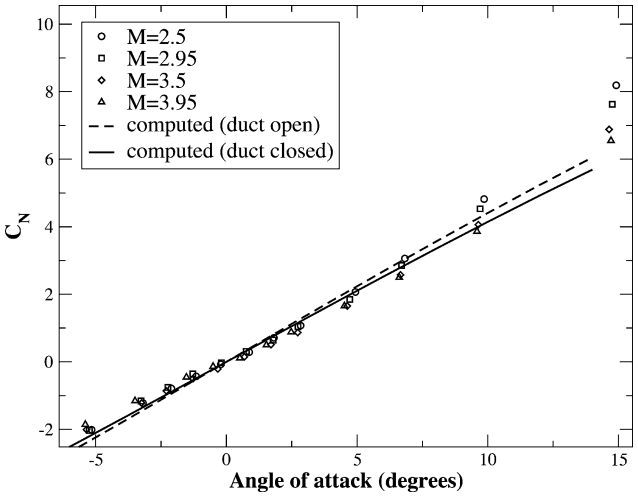

Fig. 12 Computed and experimental results for C_N vs α for the NASA B1I2T1 configuration shown in Fig. 11. The experimental results are for different supersonic Mach numbers.

vortices and therefore does not produce a significant amount of lift. The two-dimensional computation effectively treats the tail as if it were a wing extending up to the nose and hence overpredicts the lift as in the B1I1T1 case. However, in the B1I2T1 case the separation of the flow over the inlets also increases the experimental load. Hence, the excellent agreement between the computed and experimental values in this case is fortuitous.

However, for the geometries considered in this work, the technique developed does display reasonably good agreement with the experimental values for small angles of attack ($-8.0\,\text{deg} < \alpha < 8.0\,\text{deg}$). This is encouraging given the fact that the computation is very fast and easy. The computation is much easier than a full three-dimensional simulation because of the highly simplified geometry that needs to be considered. For the B1I2T1 case with 672 panels, the computation for C_N at $\alpha = 8$ deg took less than 1 s to complete on a Pentium 4 (1.7 GHz) machine. This clearly indicates that the method is very efficient.

Conclusions

In this paper a simple two-dimensional technique for the computation of the normal load on slender airbreathing bodies is presented. The analysis is subsonic and yet produces results that compare well with experimental data, which are for supersonic Mach numbers. This clearly shows that the assumption that the crossflow is responsible for the normal load is valid for airbreathing shapes at small angles of attack. The simplicity of the method makes it extremely fast. The presented results indicate that quick engineering estimates for the normal load on slender airbreathing bodies can be easily and efficiently obtained using the method developed in this work.

Acknowledgments

This work was done as part of a Defense Research and Development Laboratory (DRDL) project. The authors thank DRDL,

Hyderabad, for their support and K. Govindarajan (B. Tech. Aerospace Engineering, Indian Institute of Technology—Madras, 1999) for his work.

References

[1]Katz, J., and Plotkin, A., *Low-Speed Aerodynamics: From Wing Theory to Panel Methods*, McGraw–Hill, New York, 1991, Chap. 8.

[2]Rajan, S. C., and Shashidhar, S., "Exact Leading Term Solution for Low Aspect Ratio Wings," *Journal of Aircraft*, Vol. 34, No. 4, 1997, pp. 571–573.

[3]Champigny, P., Baudin, D., and Gonidec, P., "Prevision des Coefficients Aerodynamiques de Missiles Munis de Prises d'Air," AGARD, CP 493, Oct. 1990.

[4]Hayes, C., "Aerodynamic Characteristics of a Series of Twin-Inlet Air-Breathing Missile Configurations: 3—Axisymmetric and Two-Dimensional Inlets at Subsonic Speeds," NASA TM 84560, 1983.

[5]Hayes, C., "Aerodynamic Characteristics of a Series of Twin-Inlet Air-Breathing Missile Configurations: 1—Axisymmetric Inlets at Supersonic Speeds," NASA TM 84558, 1983.

[6]Hayes, C., "Aerodynamic Characteristics of a Series of Twin-Inlet Air-breathing Missile Configurations: 2—Two-Dimensional Inlets at Supersonic Speeds," NASA TM 84559, 1983.

[7]Roache, P. J., *Verification and Validation in Computational Science and Engineering*, Hermosa, Albuquerque, NM, 1998, p. 118.

M. Miller
Associate Editor